



UNIVERSITÀ POLITECNICA DELLE MARCHE
Repository ISTITUZIONALE

Iron(III) fate after complexation with soil organic matter in fine silt and clay fractions: An EXAFS spectroscopic approach

This is the peer reviewed version of the following article:

Original

Iron(III) fate after complexation with soil organic matter in fine silt and clay fractions: An EXAFS spectroscopic approach / Giannetta, Beatrice; Siebecker, Matthew G.; Zaccone, Claudio; Plaza, César; Rovira, Pere; Vischetti, Costantino; Sparks, Donald L.. - In: SOIL & TILLAGE RESEARCH. - ISSN 0167-1987. - ELETTRONICO. - 200:(2020). [10.1016/j.still.2020.104617]

Availability:

This version is available at: 11566/275652 since: 2024-04-24T16:41:08Z

Publisher:

Published

DOI:10.1016/j.still.2020.104617

Terms of use:

The terms and conditions for the reuse of this version of the manuscript are specified in the publishing policy. The use of copyrighted works requires the consent of the rights' holder (author or publisher). Works made available under a Creative Commons license or a Publisher's custom-made license can be used according to the terms and conditions contained therein. See editor's website for further information and terms and conditions.

This item was downloaded from IRIS Università Politecnica delle Marche (<https://iris.univpm.it>). When citing, please refer to the published version.

(Article begins on next page)

**Iron(III) fate after complexation with soil organic matter in fine silt and clay
fractions: an EXAFS spectroscopic approach**

Beatrice Giannetta ^a, Matthew G. Siebecker ^{b, c}, Claudio Zacccone ^{d, *}, César Plaza ^e, Pere
Rovira ^f, Costantino Vischetti ^g, Donald L. Sparks ^{b, h}

^a *Department of Agricultural, Forest and Food Sciences, University of Torino, Largo
Paolo Braccini 2, 10095 Grugliasco, Italy*

^b *Delaware Environmental Institute, University of Delaware, Interdisciplinary Science
and Engineering (ISE) Laboratory, 221 Academy Street, Newark, Delaware 19716, USA*

^c *Department of Plant and Soil Science, Texas Tech University, Lubbock, TX, 79409, USA*

^d *Department of Biotechnology, University of Verona, Strada Le Grazie 15, Verona,
37134, Italy*

^e *Instituto de Ciencias Agrarias, Consejo Superior de Investigaciones Científicas,
Serrano 115 bis, 28006 Madrid, Spain*

^f *Forest Science and Technology Centre of Catalonia, Carretera de St Llorenç de
Morunys, km 2, 25280 Solsona, Spain*

^g *Department of Agricultural, Food and Environmental Sciences, Polytechnic University
of Marche, via Brecce Bianche 10, 60131 Ancona, Italy*

^h *Department of Plant and Soil Sciences, University of Delaware, Interdisciplinary
Science and Engineering (ISE) Laboratory, 221 Academy Street, Newark, Delaware
19716, USA*

^{*} Corresponding author. E-mail address: claudio.zacccone@univr.it

Abstract

Iron (Fe) speciation in soils is highly dependent on environmental conditions, mineralogy, and chemical interactions with soil organic matter (SOM). The fine silt and clay (FSi+Cl) particle size fraction of soils constitutes a primary organo-mineral fraction and contains SOM with long turnover time. In this study, the FSi+Cl particle size fractions isolated from a coniferous forest, a grassland, a technosol, and an agricultural soil were reacted with Fe(III) at pH 7. Unreacted and reacted samples were then investigated by means of extended X-ray absorption fine structure (EXAFS) spectroscopy. Statistical methods were used to determine goodness-of-fit parameters for linear combination fitting (LCF) and wavelet transformation (WT) of the Fe K-edge EXAFS data. WT separated spectral contributions from different backscattering atoms in higher coordination shells located at similar interatomic distances from the central absorbing Fe atom. LCF results paired with WT showed that the FSi+Cl particle size fractions consisted of a mixture of Fe phyllosilicates, Fe (hydr)oxides, and organically complexed Fe in different proportions. Our research revealed that after sorption experiments, in which Fe(III) was added to the system, increasing amounts of organic Fe(III)-SOM complexes were found in the solid phase of grassland and agricultural soils, whereas the precipitation of Fe(III) led to the preferential formation of ferrihydrite in the coniferous forest soil and in the technosol. Although the quantitative Fe-mediated organic carbon stabilization effect after Fe(III) addition is shown in this work, Fe speciation is not clearly related to SOM amount or quality (*i.e.*, carbon-to-nitrogen ratio). The variation of Fe chemical speciation among the soil fractions likely translates into differences in their environmental fate.

Keywords: physical fractionation; Fe speciation; linear combination fitting.

Introduction

With 3,000 Pg of carbon (C) (Köchy et al., 2015), soils represent the largest C stock on the Earth's surface and play a pivotal role in regulating the global C cycle (Blanco-Canqui and Lal, 2004; Lal, 2004; Lehmann et al., 2007). Understanding soil organic C (SOC) dynamics and how it responds to soil management is extremely important especially under the current climate change scenario.

The formation of protective associations between minerals and soil organic matter (SOM) is important to prevent further release of carbon dioxide (CO₂) from soils into the atmosphere. The finer fraction of soil constituents (*i.e.*, silt and clay) is important because it contains a mixture of mineral phases with high surface area (Feng et al., 2013; Barré et al., 2014), which is an important driver of C sequestration potential in soils (Kögel-Knabner et al., 2008).

The fine silt and clay (FSi+Cl) soil fraction is characterized by the presence of multiple iron (Fe) mineral phases, ranging from Fe(II)/Fe(III) phyllosilicates to poorly or highly crystalline Fe-oxides, hydroxides, and oxyhydroxides. Fe-(hydr)oxide minerals are ubiquitous in soils (Schwertmann, 1991) and represent an important phase for the stabilization of SOC (Jambor and Dutrizac, 1998; Eusterhues et al., 2005; Lalonde et al., 2012). Fe-SOM complexation, which is affected by the nature of SOM (Rose et al., 1998), influences long-term C sequestration and can modify the reactivity and structure of Fe (hydr)oxides (Eusterhues et al., 2008, 2014). In particular, Fe oxide crystal structure is affected by coprecipitation with humic substances, which inhibits their transformation into more stable forms (*e.g.*, ferrihydrite to goethite) (Schwertmann, 1966; Schwertmann et al., 2005). Although calcium (Ca) is believed to be the main SOM stabilizer cation in the calcareous soils typical of the Mediterranean area (Giannetta et al., 2019a), Fe oxyhydroxides may be also important in the long-term stabilization of SOM (Mikutta et

al., 2006; Kögel-Knabner et al., 2008). Thus, improving our understanding about the molecular structure and hydrolysis of Fe species formed in association with SOM and the stabilization mechanisms of SOM-Fe coprecipitates is fundamental to predict the response of soil Fe and organic C to changes in global climate and land use (Post and Kwon, 2000).

Recently, state-of-the-art synchrotron-based techniques, such as Extended X-ray Absorption Fine Structure (EXAFS) spectroscopy, have been solely used for the speciation of model metal (hydr)oxide systems (pure Fe (hydr)oxides) and Fe(III) complexation with different types of SOM, including dissolved organic matter (DOM) (Nierop et al., 2002; Eusterhues et al., 2008, 2011; Henneberry et al., 2012; Chen et al., 2014), peats (Karlsson and Persson, 2010), humic substances (Mikutta and Kretzschmar, 2011; Shimizu et al., 2013), and small organic acids (Mikutta, 2011; Yang et al., 2016), in addition to bulk soils and waters (Sundman et al., 2014). In contrast, the chemical interactions between Fe species and physically-fractionated SOM pools have not been deeply investigated, and it is virtually unknown how Fe-mediated stabilization of SOM in natural rather than model systems can control the persistence of organic C as a solid phase in the soil. Thus, there is a gap between these modelled systems and natural systems, which include soils from a variety of land uses.

As an additional step to previous sorption/desorption experiments (Giannetta et al., 2019b), here we investigated, by solid phase Fe speciation, the effects of added Fe on Fe minerals and SOM contained in the FSi+Cl fraction of soils with different land use. The main objective of this study was to test the formation of Fe(III)-SOM complexes and Fe(III) precipitates as Fe(III) oxides in FSi+Cl fractions subjected to coprecipitation experiments. These products were determined via Fe speciation analysis of Fe K-edge EXAFS spectra. This important step in the research on SOM-Fe mineral complexation is

challenging because of the heterogeneity of SOM and Fe minerals naturally present in soils.

2. Materials and methods

2.1. Soil samples

The soil samples were collected from a coniferous forest (CF), a grassland (GL), a technosol (TS) and an agricultural field (AG). Mean annual temperature of sampling sites ranged from 9.7 and 14.8 °C, whereas mean annual precipitation ranged between 440 and 980 mm. The coniferous forest consisted mainly of *Pinus nigra* woodlands occurring at 630 m a.s.l., whereas the pasture, grown around 1000 m a.s.l., was dominated by meso- to xerophilous species (*e.g.*, *Bromus erectus*). The technosol consisted of a dump reclaimed in 2000, while the AG soil was an experimental field located at 530 m a.s.l. The main physical and chemical properties of soils included in this study are described elsewhere (Plaza et al., 2016; Giannetta et al., 2018, 2019b) and summarized in Table 1.

2.2. Physical fractionation

A physical size fractionation by ultrasonic dispersion and wet sieving was performed, allowing for separation of particles into four different size fractions: coarse sand (CSa: 2000-200 µm diameter), fine sand (FSa: 200-50 µm), coarse silt (CSi: 50-20 µm) and fine silt and clay (FSi+Cl: <20 µm) (Lopez-Sangil and Rovira, 2013). 15 g of each sample were put into 50 mL vials and filled with deionized water to 3/4 of their volume. Samples were then subjected to vertical agitation (20 rpm) for 60 minutes and to ultrasonic dispersion of the soil particles at an energy input of 1020 J mL⁻¹ for 10 minutes using a Branson 45 sonifier. The derived suspensions were then wet-sieved through a set of three sieves (200 µm, 50 µm and 20 µm mesh) splitting particles into four different size

fractions. The fractions retained by sieves (CSa, FSa, CSi) were quantitatively transferred to pre-weighted vials and dried at 60 °C to constant weight. The particles passing through the last sieve (<20 µm: FSi+Cl) were brought to *ca.* 1 L and left to stand refrigerated for 2 days; overlying water was then carefully siphoned off and discarded. The sediment was transferred into 250 mL polypropylene vials and centrifuged for 15 min at 2500 g and then dried at 60 °C. In this research, we used exclusively the FSi+Cl fractions, which are the fractions with the highest specific surface area and expected to be the most active with respect to organic C and Fe(III) sorption.

2.3. Characterization of FSi+Cl fractions

X-ray powder diffraction was conducted using a Philips X'Pert diffractometer with Cu K α radiation and a scan rate of 0.02° 2 θ s⁻¹. XRD patterns were collected in the 3–70° 2 θ range. The mineral composition was determined by comparison with the reference intensity ratio (RIR) values in the powder diffraction database of the International Centre for Diffraction Data (Chung, 1974a,b, 1975), using the software X'Pert HighScore 2.2e (Malvern Panalytical, Malvern, UK).

Total organic C and N contents were determined by dry combustion using a Thermo Flash 2000 NC Soil Analyzer. Each sample was ground with a ball mill and subjected to acid fumigation before analysis to remove carbonates (Harris et al., 2001). Total Fe content was determined by Inductively Coupled Plasma - Optical Emission Spectrometry (ICP-OES) after digestion with nitric and perchloric acid.

2.4. Sorption experiments

Fe(III)-SOM complexation was conducted following the methods proposed by Karlsson and Persson (2010) and Mikutta and Kretzschmar (2011) with slight modifications. In

particular, 200 mg of each fraction was weighted into a 50 mL polypropylene vial. Acidified Fe(III) nitrate stock solution (12.15 mM) was added to each sample to reach a loading of 200 mg Fe /g C. The pH of the slurry was immediately raised to 7 and monitored during the next 24 hours and adjusted to 7 ± 0.5 with 0.1 M KOH. The suspensions were shaken at 60 rpm at room temperature for 24 hours and then centrifuged at 10,000 rpm for 20 minutes. The supernatant was removed and filtered through a 0.2 μ m polysulfone membrane filter and acidified with 2% HNO₃ (trace metal grade). Filtrates were analyzed for both dissolved organic C (DOC), using a Vario TOC cube analyzer, and Fe concentration, by ICP-MS. These sorption experiments were conducted in duplicate at room temperature and the results described in Giannetta et al. (2019b).

2.5. Iron K-edge Extended X-ray Absorption Fine Structure (EXAFS) spectroscopy

The speciation of Fe in the solid phase before and after the reaction from our previous sorption study (Giannetta et al., 2019b) was analyzed by X-ray absorption spectroscopy (XAS), which generally has a beam size of ca. 10 mm². This spot size is thousands of times larger than other techniques commonly used to study SOM functional groups in a sample (Stuckey et al., 2017). XAS analyses of reacted and unreacted samples were conducted at Beamlines 4-1 and 4-3 at the Stanford Synchrotron Radiation Lightsource (SSRL) in Menlo Park (CA, USA). Fe K-edge EXAFS were collected in transmission mode. X-ray energy was maintained by a Si (222) crystal monochromator at 4-1 and Si (111) at 4-3. The monochromator was detuned 50% to reduce higher order harmonics. Ground samples (15-30 mg) were prepared as pressed pellets between Kapton® tape. Two to six replicate scans were collected in order to obtain satisfactory signal to noise ratios, with energy calibrated against an Fe (0) foil to the inflection point of the first derivative (7112 eV).

Statistical methods have been used to determine goodness-of-fit parameters for linear combination fitting (LCF) and wavelet transformation (WT). WT is useful to separate contributions from different backscattering atoms in higher coordination shells located at similar interatomic distances from the central absorbing Fe atom. A detailed description of the methods used is reported in the Supporting Information.

3. Results and Discussion

3.1. Mineralogy and elemental composition of the FSi+Cl fractions

The FSi+Cl fractions isolated from CF and GL show a similar composition in terms of both main mineral phases and relative percentages. In particular, both FSi+Cl fractions consist mainly of quartz (34-36%), calcite (19%), illite (18-19%) and microcline (10%) (Table 2). The FSi+Cl fraction isolated from TS is similar to the previous ones but shows a higher calcite content (30%) and slightly lower contents of microcline (4%) and quartz (Table 2). In contrast, the FSi+Cl fraction isolated from AG shows significant differences in terms of mineral composition, being characterized by significantly higher contents of quartz (44%), kaolinite (8%) and chlorite (6%) and a lower content of calcite (4%); moreover, muscovite (12%) occurs exclusively in this sample, whereas no montmorillonite and illite are detected (Table 2).

Organic C and total N contents of the examined fractions is shown in Table 3. Organic C content ranges from 0.7 to 8.5 g kg⁻¹, whereas total N varies between 0.08 and 0.76 g kg⁻¹. In all the cases, the lowest and the highest concentration values are found in the FSi+Cl fraction from TS and GL, respectively. The corresponding C/N ratios, ranging from 8 to 13, could point to an organic matter fraction of different origin.

Quantitative Fe speciation in FSi+Cl fractions

LCF results are reported in Table 4, revealing the standards that best reconstruct the sample data. Although Fe EXAFS provides a good estimation of the relative contribution from different Fe phases (*e.g.*, discrimination of Fe oxyhydroxides and Fe-organic complexes), it is well reported that differentiating among specific Fe(III) oxyhydroxides (*e.g.*, ferrihydrite, goethite and hematite) can be difficult (O'Day et al., 2004; Prietzel et al., 2007). Application of the F-test (Hamilton test) and use of the scree plot (Figure S1), as well as Principal Components Analysis (PCA) and Target Transformation (TT), were employed to determine the appropriate standards for LCF since the increase and decrease of only one standard can heavily influence the calculated percentage of each component (Siebecker et al., 2017). TT values are described in Table S1.

Thus, three standards were used for LCF: (1) Fe in phyllosilicates bound in the octahedral layer; (2) ferrihydrite was selected to represent pedogenic Fe(III)-minerals; and (3) Fe(III)-citrate as a model compound for organically bound Fe (O'Day et al., 2004). Fe(III)-citrate was chosen to represent Fe complexed with low-molecular weight organic acids (LMWOA), being one of the major constituents in microbial metabolites and root exudates (Yang et al., 2016) and assuming that organically bound Fe is mainly bound to carboxylate groups of deprotonated LMWOA (Pohlman and McColl, 1988; Prietzel et al., 2007). Moreover, LMWOA represent a common soil constituent, are partly redox-active, and their interaction with Fe(III)-hydroxides is comparable to that with SOM (Evanko and Dzombak, 1998).

The LCF of Fe EXAFS data of unreacted soils revealed that the ferrihydrite component varied from 23% in CF to 48% in GL, TS and AG, while Fe(III)-SOM complexes, reported as Fe(III)-citrate, ranged from 18% in GL to 41% in CF (Table 3). After the addition and precipitation of Fe(III), a small increase in ferrihydrite percentage is noticeable in CF (from 23 to 30%) and TS (from 47 to 52%), whereas in GL and AG a

reduction in ferrihydrite percentage is observed. On the other hand, the Fe(III)-citrate percentage increased in GL (from 18 to 23%) and AG (from 37 to 46%), and decreases in CF (from 41 to 35%) and TS (from 33 to 28%) (Table 4).

Fe(III)-silicates are represented by illite (39%) in CF, smectite (31%) in GL, and chlorite in TS and AG (26% and 22%, respectively). The illite reference sample contains 7.32 wt % Fe_2O_3 and 0.55 wt % FeO substituted in the octahedral layer for Al. Smectite is a low-Fe standard with 1.42% Fe_2O_3 and 0.88 wt % FeO that also contains Al and Mg in the octahedral layer (O'Day et al., 2004).

3.2. Qualitative Fe speciation in FSi+Cl fractions

LCF results are also shown in Figure 1, where the fit of each sample is represented as dotted lines and can be compared to the EXAFS spectra of the standards (Figure S2). Fe K-edge EXAFS spectra of unreacted samples show similar features at $\sim 4.0 \text{ \AA}^{-1}$ (peak 1), $\sim 6.5 \text{ \AA}^{-1}$ (peak 2), $\sim 7.5 \text{ \AA}^{-1}$ (peak 3), and $\sim 8.5 \text{ \AA}^{-1}$ (peak 4). The peak at 4.0 \AA^{-1} remained unchanged after reaction with Fe(III). Conversely, the peak at 7.5 \AA^{-1} , characteristic of ferrihydrite (Mikutta, 2011), becomes less evident in GL and AG.

The applicability of LCF to quantify different Fe phases in heterogeneous materials such as soils and different particle size fractions still represents an obstacle because often natural constituents can be only partially represented by Fe minerals synthesized in the laboratory (Prietz et al., 2007). For this reason, the LCF values often do not sum to 100%. Conversely, in model systems, such synthetic ferrihydrite, shell fitting analysis of the second-shell can be carried out because the systems are simplified. The Fe–C and Fe–Fe distances in those model systems describe the coordination modes of the organic Fe complexes and the polymeric Fe (hydr)oxides, respectively. Gustafsson et al. (2007) reported that Fe(III) in organic soils (pH 4) occurred either as Fe (hydr)oxides or

organically complexed likely as a mixture of di- and trinuclear $(\text{O}_5\text{Fe})_2\text{O}$ and $(\text{O}_5\text{Fe})_3\text{O}$ complexes. Rose et al. (1998) determined the speciation of Fe in natural organic matter (NOM) from freshwaters (pH 5.5–7.5) and found that Fe was poorly polymerized due to complexation with NOM. In our study, Fe complexation with NOM is analogous to the Fe(III)-citrate standard.

3.3. Correlation between the distribution of organic C and total N and Fe speciation in FSi+Cl fractions

There is a positive and significant correlation between the organic C and Fe content ($p < 0.05$), as well as between total N and Fe content ($p < 0.05$) (Table S2). In particular, GL and CF exhibit the highest contents of both organic C (8.5 and 5.4%, respectively) and Fe (10.3 and 9%, respectively) (Table 3) and had the lowest amount of C released into solution after the reaction at 1.8 and 1.6%, respectively (Giannetta et al., 2019b). However, there is no correlation between the Fe species and organic C and total N. The lack of significant correlation between organic C content in each soil and the Fe species means that (a) the relationship between Fe and C are either weaker than expected, (b) organic C content does not drive Fe speciation in these specific samples, or (c) a larger sample size is needed.

CF is characterized by the highest Fe(III)-SOM percentage (41%) and the lowest ferrihydrite (23%), and GL is characterized by the lowest Fe(III)-SOM percentage (18%) and the highest ferrihydrite (48%). After the reaction in CF, the precipitation of Fe(III) seems to lead to the preferential formation of ferrihydrite. This finding is in agreement with previous results reported in Giannetta et al. (2019b), who observed an increase in the carbohydrates band relative intensity in attenuated total reflectance Fourier transform infrared (ATR-FTIR) spectra after the reaction with Fe(III). This was ascribed to the

possible formation of inner-sphere surface complexes between the carbohydrate OH functional groups and the Fe atoms on the surface of ferrihydrite (*i.e.*, the formation of surface complexes between labile C sources and newly formed ferrihydrite) (Eusterhues et al., 2014, 2011). It has been shown that ferrihydrite particles can be stabilized by an encapsulating layer of polysaccharides (Karlsson and Persson, 2012). In the unreacted fraction of GL, the dominant component of Fe was present as ferrihydrite, and after the reaction a slight increase in the Fe citrate component was found. Giannetta et al. (2018) hypothesized that SOM in TS is enriched in newly formed organic molecules (*e.g.*, sugars, amino acids, proteins), mainly resulting from microbial transformation rather than in highly degraded litter inputs. These labile compounds can associate with mineral surfaces (*e.g.*, Fe(III) that precipitates as Fe(III) hydroxides) in the same way described for CF. For the AG soil, previously reported ATR-FTIR results demonstrated that small differences in carbohydrates peaks can be indicative of labile SOM associated with minerals as well as the formation of Fe-SOM complexes (Giannetta et al., 2019b); this was also discussed by Karlsson and Persson (2012) and is in agreement with the increase in Fe(III)-SOM in AG and the decrease in ferrihydrite.

Organic functional groups (ligands) found in SOM can also impact Fe mineral cycling. Ligand-promoted dissolution at neutral pH can have a large impact on Fe speciation in soils because they affect ferrihydrite formation and can exert a strong influence on its structure (Mikutta et al., 2008). Mikutta et al. (2010) reported that organic chelates such as hydroxybenzoic acids control the kinetics of ferrihydrite formation via Fe(III) complexation, thereby effectively lowering the solution saturation state of inorganic Fe(III) species, leaving less Fe(III) available for ferrihydrite precipitation. This has been demonstrated in laboratory systems and likely also occurs in soils.

3.4. Wavelet analysis of higher coordination shells

As in EXAFS studies on Fe associated with SOM, the application of traditional EXAFS analyses (*e.g.*, shell fitting of the Fourier transform; FT) can be challenging to identify specific species in heterogeneous systems such as soils; thus we also employed WT to aid in discriminating scattering elements. This challenge is due to the need to separate contributions from different backscattering atoms in coordination shells at similar interatomic distances from the central absorbing Fe atom. WT can provide useful information to simultaneously resolve data in both k -space (\AA^{-1}) and interatomic distance (R -space, \AA), helping to differentiate lighter backscattering elements when they are in the same coordination shell from the central adsorbing atom (*e.g.*, Fe *vs.* C) (Funke et al., 2005, 2007). WT represents an analogue to the FT and reveals the energies at which the backscattering components are most significant in addition to the distances of the backscattering atoms. WT k - R maps are helpful in improving the fitting model and understanding local atomic structure (Xia et al., 2018). In a parallel experiment (Giannetta et al., submitted) we applied this approach, pairing LCF and WT to illustrate the role played by organic inputs (*i.e.*, biochar and compost) to determine Fe speciation and distribution in an agricultural soil. Here, WT analysis has been used to qualitatively test for the presence of Fe backscatterers in the second coordination shell of the Fe K-edge EXAFS data. We calculated the Morlet wavelet transforms of k^3 -weighted Fe K-edge EXAFS spectra of the samples over a $R + \Delta R$ -range of 2.2-4.0 \AA (*i.e.*, the second coordination shell) and compared the resulting wavelet plots with those of Fe(III) reference compounds (ferrihydrite, Fe(III)-citrate, illite, smectite, and chlorite).

Figure 2 contains the WT plots of the standards, whereas Figure 3 displays the WT plots of the reacted and non-reacted samples. In the ferrihydrite plot, the Fe shell contributes a strong feature at 7-8 \AA^{-1} and 2.75 \AA , corresponding to the second peak in

the FT (Daugherty et al., 2017). In Fe(III)-SOM spectra (Fe-citrate) there is no Fe backscattering, but features at 2.0–2.5 Å indicate back-scattering from lighter atoms. These features are in agreement with single and multiple backscattering from C/O (Persson and Axe, 2005; Karlsson et al., 2008; Karlsson and Persson, 2010; Daugherty et al., 2017). Moreover, these features appear at lower energies (3–4 Å⁻¹) than those of Fe. The illite plot presents a strong feature at 8 Å⁻¹ and 2.8 Å (O'Day et al., 2004), similar to the ferrihydrite. This peak, however, is very weak in the chlorite and smectite WT plots, as compared to illite and ferrihydrite. The illite sample has 7.32 wt% Fe₂O₃ and 0.55 wt% FeO, presumably substituted in the octahedral layer for Al. The smectite is a low Fe variety with 1.42 wt% Fe₂O₃ and 0.08 wt% FeO, that contains mostly Al and Mg in the octahedral layer (O'Day et al., 2004). Thus, due to the lower total Fe content, the second-neighbour backscattering is lower in amplitude for smectite rather than for illite. The lack of an intense maximum in WT plots of the smectite and chlorite standards is related to their less intense second shell peak in the FT (Figure S3). In general, the first two major shells in phyllosilicate clay minerals can be described by three interatomic backscattering paths: (1) the first-neighbour O, (2) second-neighbour octahedral Fe, Al, or Mg; and (3) tetrahedral Si (Figures 2 and S3). In many Fe oxyhydroxides and phyllosilicates, the Fe-Fe neighbour distances overlap at 2.75 Å, thus the analysis of the second coordination shell is particularly complicated.

WT of the EXAFS data from the samples and the FT spectra in Figure S4 showed that the features ascribed to light backscatterers at low k-values and by heavier atoms at higher k varied among the unreacted and Fe(III) reacted samples (Figure 3). The WT plot of the unreacted CF sample indicates a Fe-Fe shell contribution similar to both ferrihydrite and illite. A contribution from Fe(III)-citrate at 2.2 Å and 2–4 Å⁻¹ is also evident, supporting the LCF results (41% of Fe(III)-citrate). The plot of the CF reacted sample

displays features typical of ferrihydrite, which increased from 23% to 30% according to the LCF result. The Fe-Fe scattering feature in unreacted GL appears at the distance in both k- and R-space ascribed to ferrihydrite. According to LCF results, GL contained the lowest Fe-citrate percentage, thus no features from C backscattering are evident in the WT plot. At $\eta = 8$, differences between unreacted and reacted samples are not evident. However, at $\eta = 6$ (Figure S6b), in the reacted GL sample, a feature at 2.2 Å appears and it is related to C backscattering. The TS WT plot shows a clear indication of heavy element back-scattering atoms. Noticeable differences are not seen in the reacted plot. In AG, the presence of 37% of Fe(III)-SOM from LCF is supported by the presence of the Fe(III)-SOM feature at 2.2 Å and 2–4 Å⁻¹. After the reaction this feature increases, as the Fe(III)-citrate increases up to 46%, in agreement with the results reported in LCF. Moreover, the same peak at 2.2 Å is increasing in the FT spectrum displayed in Figure S4.

When modifying η from 9 to 4 for both the standards (Figure S5) and the samples (Figure S6a-d), at 6, the maximum starts to separate into separate peaks, indicating the splitting of the major component into two minor components.

The second shell of phyllosilicate clay minerals results from the scattering path from different elements (as discussed above in this section); and this separation seen in the WT plots can be ascribed to the second-neighbour octahedral Fe, Al, or Mg, and tetrahedral Si, the splitting in two different components being a common feature of illite and smectite (Figures S5 and S6). In AG the splitting into separate peaks at $\eta = 6$ is not as strong (Figure S6d), as in the other samples, being AG characterized by low chlorite percentages, both in unreacted (22%) and reacted (14%) samples.

These results also highlight that WT interpretation is challenging due to the overlapping of the Fe-Fe neighbour distances in many Fe oxyhydroxides and phyllosilicates.

However, the WT results indicated that the second shell of reacted samples consisted of either lighter scattering elements such as C/O atoms and/or heavier scattering elements, such as Fe. Our data indicate that the formation of Fe(III)-SOM complexes in soils with more labile organic C may perhaps suppress the hydrolysis and polymerization of Fe(III). These complexes have different reactivity as compared to Fe(III) in (hydr)oxide phases or other Fe(III)-bearing minerals. Lastly, the WT results support the LCF analysis, which indicated that EXAFS spectra of the soil samples could be described as a mixture of Fe-bearing clay minerals, Fe (hydr)oxides and organically complexed Fe.

4. Conclusions

Here we identify how SOM can influence Fe(III) speciation by adding Fe(III) to the silt and clay fraction of different soils, and we demonstrate how both Fe(III)-SOM complexes and Fe(III) polymerization (*i.e.*, the formation of iron oxyhydroxides) can vary between each sample. Additionally, changes in SOM reactivity in these samples was previously identified, which has consequences for SOM stabilization in FSi+Cl fractions; for example, adding Fe(III) changed Fe speciation and decreased soluble DOC (Giannetta et al., 2019b). We underline the importance of pairing LCF with WT to resolve data in both k-space (energy) and interatomic distance (R-space), helping to differentiate lighter backscattering elements when they are in the same coordination shell from the central adsorbing Fe atom.

Batch sorption data from our past work (Giannetta et al., 2019b) have been used to probe the effect of different natural ecosystems on Fe(III) precipitation and complexation mechanisms. In a second step, here, both LCF and WT results indicated that the soil samples can be described as a mixture of Fe-bearing phyllosilicate clay minerals, Fe (hydr)oxides, and organically complexed Fe. Our research has revealed that after sorption

experiments in which Fe(III) was added to the system, increasing amounts of organic Fe(III)-SOM complexes in the solid phase of GL and AG soils were found; on the other hand, in the FSi+Cl fractions of the CF and TS soils, the precipitation of Fe(III) lead to the preferential formation of ferrihydrite. Finally, although the quantitative Fe-mediated organic C stabilization effect after Fe(III) addition was previously demonstrated (Giannetta et al., 2019b), the Fe speciation is not clearly related to SOM amount and C/N ratio.

In conclusion, the combination of Fe EXAFS with size-fractionated samples represents an important approach to study Fe dynamics in natural environments, as it helps unravel links among Fe originally present in the soil, formation mechanisms of different Fe species (either organically bound Fe or Fe-oxides), and the structures of those species.

Future investigations should focus on the influence of SOM on Fe speciation and complexation during changing environmental conditions (mainly redox potential and pH) and land use (*e.g.*, forest *vs.* agricultural soil). In particular, although the present study underlines different organic C sequestration potential among finer fractions isolated from soils under diverse land uses, a larger number of samples should be investigated in order to validate this hypothesis and avoid an over-interpretation of the spectroscopic results. In fact, the differences observed in our study in terms of Fe(III)-SOM formation could also be potentially related to the differences in organic ligands and mineralogy characterizing each of the studied soils, as both contribute to the binding energy of SOM (Newcomb et al., 2017).

Declaration of Competing Interest

The authors declare that they have no known competing financial interests or personal relationships that could have appeared to influence the work reported in this paper.

425

426 **Appendix A. Supplementary data**

427 The following is Supplementary data to this article: ...

428

429

430 **Acknowledgements**

431 This research was supported in part by the National Science Foundation Experimental
432 Program to Stimulate Competitive Research grant number EPS-0814251. Use of the
433 Stanford Synchrotron Radiation Lightsource is supported by the U.S. Department of
434 Energy under contract No. DE-AC02-76SF00515. C.P. acknowledges support from the
435 Spanish State Plan for Scientific and Technical Research and Innovation (2013-2016),
436 award ref. AGL201675762-R (AEI/FEDER, UE). The authors thank Miguel Juanco,
437 Materials Characterization Service (ICA-CSIC), for XRD analysis.

438

References

- Amundson, R., Berhe, A.A., Hopmans, J.W., Olson, C., Sztein, A.E., Sparks, D.L., 2015. Soil and human security in the 21st century. *Science* 348, 647–653. <https://doi.org/10.1126/science.1261071>
- Barré, P., Fernandez-Ugalde, O., Virto, I., Velde, B., Chenu, C., 2014. Impact of phyllosilicate mineralogy on organic carbon stabilization in soils: Incomplete knowledge and exciting prospects. *Geoderma* 235–236, 382–395. <https://doi.org/10.1016/j.geoderma.2014.07.029>
- Blanco-Canqui, H., Lal, R., 2004. Mechanisms of carbon sequestration in soil aggregates. *CRC. Crit. Rev. Plant Sci.* 23, 481–504. <https://doi.org/10.1080/07352680490886842>
- Chen, C., Dynes, J.J., Wang, J., Karunakaran, C., Sparks, D.L., 2014a. Soft X-ray spectromicroscopy study of mineral-organic matter associations in pasture soil clay fractions. *Environ. Sci. Technol.* 48, 6678–6686. <https://doi.org/10.1021/es405485a>
- Chen, C., Dynes, J.J., Wang, J., Sparks, D.L., 2014b. Properties of Fe-organic matter associations via coprecipitation versus adsorption. *Environ. Sci. Technol.* 48, 13751–13759. <https://doi.org/10.1021/es503669u>
- Chung, F.H., 1974a. Quantitative interpretation of X-ray diffraction patterns of mixtures. I. Matrix-flushing method for quantitative multicomponent analysis. *J. Appl. Cryst.* 7, 519–525.
- Chung, F.H., 1974b. Quantitative interpretation of X-ray diffraction patterns of mixtures. II. Adiabatic principle of X-ray diffraction analysis of mixtures. *J. Appl. Cryst.* 7, 526–531.
- Chung, F.H., 1975. Quantitative interpretation of X-ray diffraction patterns of mixtures. III. Simultaneous determination of a set of reference intensities. *J. Appl. Cryst.* 8,

17-19.

- Daugherty, E.E., Gilbert, B., Nico, P.S., Borch, T., 2017. Complexation and Redox Buffering of Iron(II) by Dissolved Organic Matter. *Environ. Sci. Technol.* 51, 11096–11104. <https://doi.org/10.1021/acs.est.7b03152>
- Eusterhues, K., Hädrich, A., Neidhardt, J., Küsel, K., Keller, T.F., Jandt, K.D., Totsche, K.U., 2014. Reduction of ferrihydrite with adsorbed and coprecipitated organic matter: Microbial reduction by *Geobacter bremensis* vs. abiotic reduction by Na-dithionite. *Biogeosciences* 11, 4953–4966. <https://doi.org/10.5194/bg-11-4953-2014>
- Eusterhues, K., Rennert, T., Knicker, H., Kögel-Knabner, I., Totsche, K.U., Schwertmann, U., 2011. Fractionation of organic matter due to reaction with ferrihydrite: Coprecipitation versus adsorption. *Environ. Sci. Technol.* 45, 527–533. <https://doi.org/10.1021/es1023898>
- Eusterhues, K., Rumpel, C., Kögel-Knabner, I., 2005. Stabilization of soil organic matter isolated via oxidative degradation. *Org. Geochem.* 36, 1567–1575. <https://doi.org/10.1016/j.orggeochem.2005.06.010>
- Eusterhues, K., Wagner, F.E., Häusler, W., Hanzlik, M., Knicker, H., Totsche, K.U., Kögel-Knabner, I., Schwertmann, U., 2008. Characterization of Ferrihydrite-Soil Organic Matter Coprecipitates by X-ray Diffraction and Mössbauer Spectroscopy. *Environ. Sci. Technol.* 42, 7891–7897. <https://doi.org/10.1021/es800881w>
- Evanko, C.R., Dzombak, D.A., 1998. Influence of structural features on sorption of NOM-analogue organic acids to goethite. *Environ. Sci. Technol.* 32, 2846–2855. <https://doi.org/10.1021/es980256t>
- Feng, W., Plante, A.F., Six, J., 2013. Improving estimates of maximal organic carbon stabilization by fine soil particles. *Biogeochemistry* 112, 81–93.

489 <https://doi.org/10.1007/s10533-011-9679-7>

490 Funke, H., Chukalina, M., Scheinost, A.C., 2007. A new FEFF-based wavelet for EXAFS
 491 data analysis. *J. Synchrotron Radiat.* 14, 426–432.
 492 <https://doi.org/10.1107/S0909049507031901>

493 Funke, H., Scheinost, A.C., Chukalina, M., 2005. Wavelet analysis of extended x-ray
 494 absorption fine structure data. *Phys. Rev. B* 71, 094110.
 495 <https://doi.org/10.1103/PhysRevB.71.094110>

496 Giannetta, B., Plaza, C., Siebecker, M.G., Aquilanti, G., Vischetti, C., Plaisier, J.R.,
 497 Juanco, M., Sparks, D.L., Zacccone, C. (submitted). Iron speciation in organic matter
 498 fractions isolated from soils amended with biochar and organic fertilizers. *Environ.*
 499 *Sci. Technol.*

500 Giannetta, B., Plaza, C., Vischetti, C., Cotrufo, M.F., Zacccone, C., 2018. Distribution and
 501 thermal stability of physically and chemically protected organic matter fractions in
 502 soils across different ecosystems. *Biol. Fertil. Soils* 1–11.
 503 <https://doi.org/10.1007/s00374-018-1290-9>

504 Giannetta, B., Plaza, C., Zacccone, C., Vischetti, C., Rovira, P., 2019a. Ecosystem type
 505 effects on the stabilization of organic matter in soils: Combining size fractionation
 506 with sequential chemical extractions. *Geoderma* 353, 423-434.
 507 <https://doi.org/10.1016/j.geoderma.2019.07.009>

508 Giannetta, B., Zacccone, C., Plaza, C., Siebecker, M.G., Rovira, P., Vischetti, C., Sparks,
 509 D.L., 2019b. The role of Fe(III) in soil organic matter stabilization in two size
 510 fractions having opposite features. *Sci. Total Environ.* 653, 667-674.
 511 <https://doi.org/10.1016/j.scitotenv.2018.10.361>

512 Gustafsson, J.P., Persson, I., Kleja, D.B., Van Schaik, J.W.J., 2007. Binding of iron(III)
 513 to organic soils: EXAFS spectroscopy and chemical equilibrium modeling. *Environ.*

514 Sci. Technol. 41, 1232–1237. <https://doi.org/10.1021/es0615730>

515 Harris, D., Horwáth, W. R., van Kessel, C., 2001. Acid fumigation of soils to remove
516 carbonates prior to total organic carbon or carbon-13 isotopic analysis. Soil Sci. Soc.
517 Am. J. 65, 1853-1856. <https://doi.org/10.2136/sssaj2001.1853>

518 Henneberry, Y.K., Kraus, T.E.C., Nico, P.S., Horwath, W.R., 2012. Structural stability
519 of coprecipitated natural organic matter and ferric iron under reducing conditions.
520 Org. Geochem. 48, 81–89. <https://doi.org/10.1016/j.orggeochem.2012.04.005>

521 Jambor, J.L., Dutrizac, J.E., 1998. Occurrence and Constitution of Natural and Synthetic
522 Ferrihydrite, a Widespread Iron Oxyhydroxide. Chem. Rev. 98, 2549–2585.
523 <https://doi.org/10.1021/cr970105t>

524 Karlsson, T., Persson, P., 2012. Complexes with aquatic organic matter suppress
525 hydrolysis and precipitation of Fe(III). Chem. Geol. 322–323, 19–27.
526 <https://doi.org/10.1016/j.chemgeo.2012.06.003>

527 Karlsson, T., Persson, P., 2010. Coordination chemistry and hydrolysis of Fe(III) in a peat
528 humic acid studied by X-ray absorption spectroscopy. Geochim. Cosmochim. Acta
529 74, 30–40. <https://doi.org/10.1016/j.gca.2009.09.023>

530 Karlsson, T., Persson, P., Skyllberg, U., Mörth, C.-M., Giesler, R., 2008. Characterization
531 of Iron(III) in Organic Soils Using Extended X-ray Absorption Fine Structure
532 Spectroscopy. Environ. Sci. Technol. 42, 5449–5454.
533 <https://doi.org/10.1021/es800322j>

534 Köchy, M., Hiederer, R., Freibauer, A., 2015. Global distribution of soil organic carbon
535 – Part 1: Masses and frequency distributions of SOC stocks for the tropics,
536 permafrost regions, wetlands, and the world. Soil 1, 351–365.
537 <https://doi.org/10.5194/soil-1-351-2015>

538 Kögel-Knabner, I., Guggenberger, G., Kleber, M., Kandeler, E., Kalbitz, K., Scheu, S.,

- Eusterhues, K., Leinweber, P., 2008. Organo-mineral associations in temperate soils: Integrating biology, mineralogy, and organic matter chemistry. *J. Plant Nutr. Soil Sci.* 171, 61–82. <https://doi.org/10.1002/jpln.200700048>
- Lal, R., 2004. Soil carbon sequestration to mitigate climate change. *Geoderma* 123, 1–22. <https://doi.org/10.1016/j.geoderma.2004.01.032>
- Lalonde, K., Mucci, A., Ouellet, A., G  linas, Y., 2012. Preservation of organic matter in sediments promoted by iron. *Nature* 483, 198–200. <https://doi.org/10.1038/nature10855>
- Lehmann, J., Kinyangi, J., Solomon, D., 2007. Organic matter stabilization in soil microaggregates: Implications from spatial heterogeneity of organic carbon contents and carbon forms. *Biogeochemistry* 85, 45–57. <https://doi.org/10.1007/s10533-007-9105-3>
- Lopez-Sangil, L., Rovira, P., 2013. Sequential chemical extractions of the mineral-associated soil organic matter: An integrated approach for the fractionation of organo-mineral complexes. *Soil Biol. Biochem.* 62, 57–67. <https://doi.org/10.1016/j.soilbio.2013.03.004>
- Mikutta, C., 2011. X-ray absorption spectroscopy study on the effect of hydroxybenzoic acids on the formation and structure of ferrihydrite. *Geochim. Cosmochim. Acta* 75, 5122–5139. <https://doi.org/10.1016/j.gca.2011.06.002>
- Mikutta, C., Frommer, J., Voegelin, A., Kaegi, R., Kretzschmar, R., 2010. Effect of citrate on the local Fe coordination in ferrihydrite, arsenate binding, and ternary arsenate complex formation. *Geochim. Cosmochim. Acta* 74, 5574–5592. <https://doi.org/10.1016/j.gca.2010.06.024>
- Mikutta, C., Kretzschmar, R., 2011. Spectroscopic evidence for ternary complex formation between arsenate and ferric iron complexes of humic substances. *Environ.*

564 Sci. Technol. 45, 9550–9557. <https://doi.org/10.1021/es202300w>
 565 Mikutta, C., Mikutta, R., Bonneville, S., Wagner, F., Voegelin, A., Christl, I.,
 566 Kretzschmar, R., 2008. Synthetic coprecipitates of exopolysaccharides and
 567 ferrihydrite. Part I: Characterization. *Geochim. Cosmochim. Acta* 72, 1111–1127.
 568 <https://doi.org/10.1016/j.gca.2007.11.035>
 569 Newcomb, C.J., Qafoku, N.P., Grate, J.W., Bailey, V.L., De Yoreo, J.J., 2017.
 570 Developing a molecular picture of soil organic matter–mineral interactions by
 571 quantifying organo–mineral binding. *Nat. Commun.* 8, 396.
 572 <https://doi.org/10.1038/s41467-017-00407-9>
 573 Nierop, K.G.J., Jansen, B., Verstraten, J.M., 2002. Dissolved organic matter, aluminium
 574 and iron interactions: Precipitation induced by metal/carbon ratio, pH and
 575 competition. *Sci. Total Environ.* 300, 201–211. <https://doi.org/10.1016/S0048->
 576 9697(02)00254-1
 577 O'Day, P.A., Rivera, N., Root, R., Carroll, S.A., 2004. X-ray absorption spectroscopic
 578 study of Fe reference compounds for the analysis of natural sediments. *Am. Mineral.*
 579 89, 572–585. <https://doi.org/10.2138/am-2004-0412>
 580 Persson, P., Axe, K., 2005. Adsorption of oxalate and malonate at the water-goethite
 581 interface: Molecular surface speciation from IR spectroscopy. *Geochim.*
 582 *Cosmochim. Acta* 69, 541–552. <https://doi.org/10.1016/j.gca.2004.07.009>
 583 Pohlman, A.A., McColl, J.G., 1988. Soluble Organics from Forest Litter and their Role
 584 in Metal Dissolution. *Soil Sci. Soc. Am. J.* 52, 265–271.
 585 <https://doi.org/10.2136/sssaj1988.03615995005200010047x>
 586 Post, W.M., Kwon, K.C., 2000. Soil carbon sequestration and land-use change : processes
 587 and potential. *Glob. Chang. Biol.* 6, 317–327. <https://doi.org/10.1046/j.1365->
 588 2486.2000.00308.x

- Prietz, J., Thieme, J., Eusterhues, K., Eichert, D., 2007. Iron speciation in soils and soil aggregates by synchrotron-based X-ray microspectroscopy (XANES, μ -XANES). *Eur. J. Soil Sci.* 58, 1027–1041. <https://doi.org/10.1111/j.1365-2389.2006.00882.x>
- Rose, J., Vilge, A., Olivie-Lauquet, G., Masion, A., Frechou, C., Bottero, J.Y., 1998. Iron speciation in natural organic matter colloids. *Colloids Surfaces A Physicochem. Eng. Asp.* 136, 11–19. [https://doi.org/10.1016/S0927-7757\(97\)00150-7](https://doi.org/10.1016/S0927-7757(97)00150-7)
- Schwertmann, U., 1991. Solubility and dissolution of iron oxides. *Plant Soil*, 130, 1–25. https://doi.org/10.1007/978-94-011-3294-7_1
- Schwertmann, U., 1966. Inhibitory effect of soil organic matter on the crystallization of amorphous ferric hydroxides. *Nature*, 209, 645–646. <https://doi.org/10.1038/212645b0>
- Schwertmann, U., Wagner, F., Knicker, H., 2005. Ferrihydrite–Humic Associations. *Soil Sci. Soc. Am. J.* 69, 1009. <https://doi.org/10.2136/sssaj2004.0274>
- Shimizu, M., Zhou, J., Schröder, C., Obst, M., Kappler, A., Borch, T., 2013. Dissimilatory reduction and transformation of ferrihydrite-humic acid coprecipitates. *Environ. Sci. Technol.* 47, 13375–13384. <https://doi.org/10.1021/es402812j>
- Siebecker, M.G., Chaney, R.L., Sparks, D.L., 2017. Nickel speciation in several serpentine (ultramafic) topsoils via bulk synchrotron-based techniques. *Geoderma* 298, 35–45. <https://doi.org/10.1016/j.geoderma.2017.03.008>
- Stuckey, J.W., Yang, J., Wang, J., Sparks, D.L., 2017. Advances in Scanning Transmission X-Ray Microscopy for Elucidating Soil Biogeochemical Processes at the Submicron Scale. *J. Environ. Qual.* 46, 1166–1174. <https://doi.org/10.2134/jeq2016.10.0399>
- Sundman, A., Karlsson, T., Laudon, H., Persson, P., 2014. XAS study of iron speciation in soils and waters from a boreal catchment. *Chem. Geol.* 364, 93–102.

614 <https://doi.org/10.1016/j.chemgeo.2013.11.023>

615 Xia, Z., Zhang, H., Shen, K., Qu, Y., Jiang, Z., 2018. Wavelet analysis of extended X-ray

616 absorption fine structure data: Theory, application. *Phys. B Condens. Matter* 542,

617 12–19. <https://doi.org/10.1016/j.physb.2018.04.039>

618 Yang, J., Wang, J., Pan, W., Regier, T., Hu, Y., Rumpel, C., Bolan, N., Sparks, D., 2016.

619 Retention Mechanisms of Citric Acid in Ternary Kaolinite-Fe(III)-Citrate Acid

620 Systems Using Fe K-edge EXAFS and L3,2-edge XANES Spectroscopy. *Sci. Rep.*

621 6, 1–9. <https://doi.org/10.1038/srep26127>

Figure captions

Figure 1.

k^3 -weighted EXAFS spectra of fine silt and clay (FSi+Cl) fractions from coniferous forest (CF), grassland (GL), technosol (TS) and agricultural (AG) soils before (U) and after (R) reaction with Fe(III). Solid lines indicate the sample data, whereas red dotted lines represent the LCF fit.

Figure 2.

High resolution WT plots of standards displaying the second coordination shell. Data are plotted as a function of k (\AA^{-1}) on the x axis and R (\AA) on the y axis in the range 2.0-4.0 (\AA).

Figure 3.

High resolution WT plots of fine silt and clay (FSi+Cl) fractions from coniferous forest (CF), grassland (GL), technosol (TS) and agricultural (AG) soils before (U) and after (R) reaction with Fe(III) displaying the second shell. Data are plotted as a function of k (\AA^{-1}) on the x axis and R (\AA) on the y axis in the range 2.2-4.0 (\AA).

640 **Table 1.** Site details and main physical and chemical properties of the coniferous forest (CF), grassland (GL), technosols (TS) and agricultural
641 (AG) soils included in this study. Data are from Giannetta et al. (2018, 2019b).

Sample	CF	GL	TS	AG
Site	San Lorenzo (San Severino Marche, Italy)	Forcatura (Fiuminata, Italy)	Asola (Potenza Picena, Italy)	Arganda del Rey (Madrid, Spain)
Coordinates	13°14'03" E; 43°18'05" N	12°53'49" E; 43°08'51" N	13°14'49" E; 43°13'34" N	3°29'06" W; 40°18'58" N
Depth (cm)	0-25	0-15	0-20	0-15
Soil Taxonomy	Lithic Rendoll	Typic Haplustoll	-	Xerofluvent
Land use	Reforestation with <i>Pinus nigra</i> (dominant species); age: 60 years	Natural or semi-natural meadows and pastures	Dump reclaimed in 2000	Unamended, agricultural soil, planted with <i>Hordeum vulgare</i>
pH	7.9	7.6	8.5	8.4
Sand ($g \cdot kg^{-1}$)	527	631	142	339
Silt ($g \cdot kg^{-1}$)	212	202	452	471
Clay ($g \cdot kg^{-1}$)	261	167	406	190
Organic C ($g \cdot kg^{-1}$)	77.9	93.0	7.5	11.8
Total N ($g \cdot kg^{-1}$)	4.5	7.7	0.8	1.1
C/N	17.4	12	9	10.7
Fe ($g \cdot kg^{-1}$)	30.9	27.5	21.2	22.1

642

643 **Table 2.** Mineralogical composition of the fine silt plus clay (FSi+Cl) fraction isolated
644 from a coniferous forest soil (CF), a grassland soil (GL), a technosol (TS) and an
645 agricultural soil (AG).

646

PDF ref. number	Compound name	CF FSi+Cl	GL FSi+Cl	TS FSi+Cl	AG FSi+Cl
<i>SemiQuant [%]</i>					
00-013-0259	Montmorillonite	2	4	2	-
00-043-0685	Illite	19	18	16	-
01-086-1384	Muscovite	-	-	-	12
01-080-0885	Kaolinite	4	3	4	8
01-072-1234	Chlorite	3	3	3	6
01-085-0798	Quartz	36	34	31	44
01-084-1455	Microcline	10	10	4	13
01-076-0927	Albite	7	9	9	11
01-081-2027	Calcite	19	19	30	4
01-083-1766	Dolomite	-	-	1	2

647

Table 3. Chemical properties of the fine silt and clay (FSi+Cl) fractions isolated from a coniferous forest soil (CF), a grassland soil (GL), a technosol (TS) and an agricultural soil (AG).

	Organic C (%)	Total N (%)	C/N	Fe (%)
CF FSi+Cl	5.4	0.42	12.9	9.0
GL FSi+Cl	8.5	0.76	11.1	10.3
TS FSi+Cl	0.7	0.08	8.2	7.4
AG FSi+Cl	1.8	0.19	9.5	8.5

Table 4. Summary of EXAFS linear combination fitting of fine silt and clay (FSi+Cl) fractions from coniferous forest (CF), grassland (GL), technosol (TS) and agricultural (AG) soils before (U) and after (R) reaction with Fe(III) over the k range 2.5-10 Å. F-test has been calculated and is reported in column “I”. It denotes the fit improvement using three standards instead of two.

FSi+Cl sample	k range fit	I	Measurements	R-factor	Component 1 Fe-silicates	Component 2 Ferrihydrite	Component 3 Fe(III) citrate	Sum	
CF U	2.5-9	0.248	13.414	0.0086	Illite	39%	23%	41%	102%
CF R	2.5-10	0.013	14.369	0.0178	Illite	25%	30%	35%	90%
GL U	2.5-10	0.002	15.324	0.0266	Smectite	31%	48%	18%	97%
GL R	2.5-10	0.001	15.324	0.0387	Smectite	21%	43%	23%	86%
TS U	2.5-10	0.050	15.324	0.0729	Chlorite	26%	47%	33%	105%
TS R	2.5-10	0.025	15.324	0.0959	Chlorite	33%	52%	28%	112%
AG U	2.5-10	0.002	15.324	0.0320	Chlorite	22%	48%	37%	107%
AG R	2.5-10	0.021	15.324	0.0604	Chlorite	14%	41%	46%	102%

Figure 1.

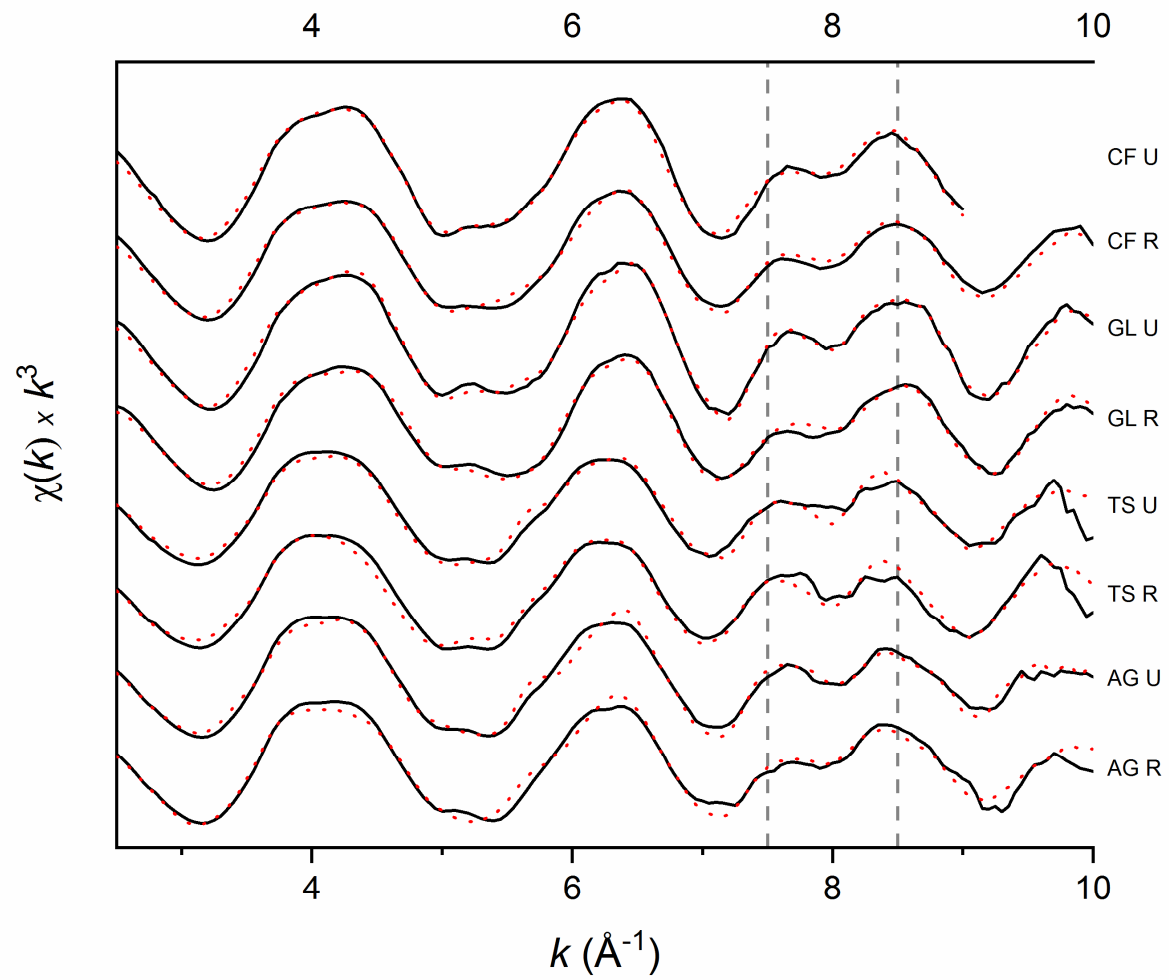


Figure 2.

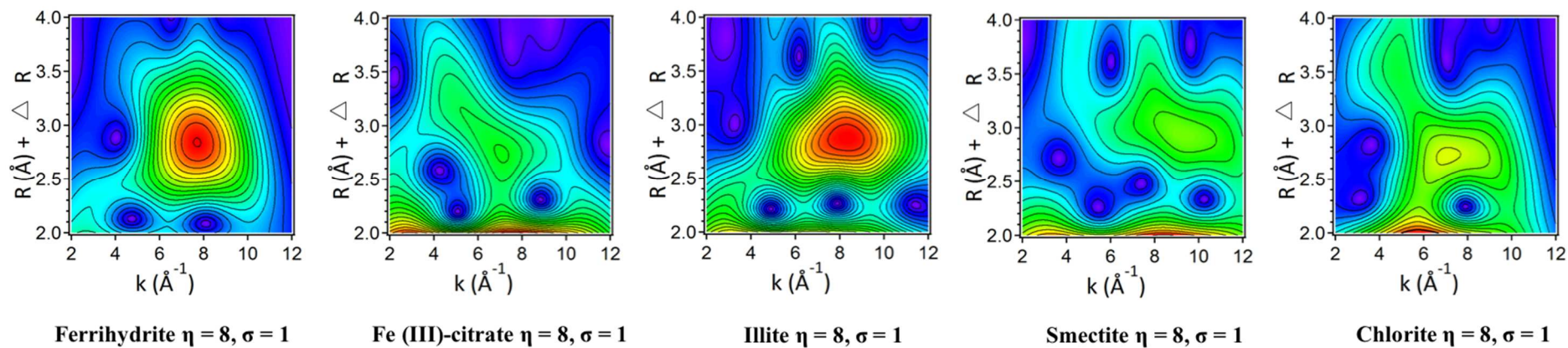


Figure 3.

